1. INTRODUCTION AND SIGNFICANCE OF THE RESEARCH

Quantum computing is one of the most important current areas of research. As quantum information is still in its infancy, there are many approaches to a possible quantum computer [1]: nonlinear optics, ion traps, superconducting qubits, ultacold atoms in optical lattices, quantum dots … Since Bose-Einstein condensates (BECs) exhibit quantum effects at a macroscopic level, they appear to be an excellent springboard for quantum information processing. Moreover, in the BEC ground state all the bosons occupy the same (single particle) wave function whose mean-field evolution is given by the Gross-Pitaevskii (GP) equation [2] (which in nonlinear optics is known as the nonlinear Schrodinger equation[NLS]). Here, we propose to study the unitary **q**uantum **l**attice **g**as (QLG) algorithm [3] for spinor-BECs [4] as two component BECs can be used in the encoding of quantum information [1]. Interestingly, these two-component BECs can be manipulated in the same way as qubits – with qubits forming the backbone of our QLG algorithm.

A qubit is a superposition of two possible states of a system: which we can denote by, say, $|0\rangle$ and $|1\rangle$. The local quantum entanglement of 2 qubits/site takes the form

$$|q_1 q_2\rangle = \alpha_{00}|00\rangle + \alpha|01\rangle + \beta|10\rangle + \alpha_{11}|11\rangle. \tag{1}$$

Scalar QLG algorithms described here perform a particular unitary collide-stream sequence of operations on the spinor field probability amplitudes α, β in Eq. (1):

$$|\psi(t)\rangle = \begin{pmatrix} \alpha \\ \beta \end{pmatrix} \tag{2}$$

- the particular sequence of unitary operators being dependent on the desired macroscopic level physics under study. (This chosen sequence, of course, is not necessarily unique). Our earlier 1D QLG algorithms have been successfully benchmarked against the exact soliton solutions of the 1D nonlinear Schrodinger (NLS) equation [5] – with its extension to inelastic vector soliton collisions [6] – and the Korteweg-de Vries (KdV) [5] equation. For the QLG representation of 1D NLS:

NLS: $\quad i\dfrac{\partial \psi}{\partial t} = -\dfrac{\partial^2 \psi}{\partial x^2} - |\psi|^2 \psi \qquad\qquad$ [bright soliton] $\qquad$ (3)

we [5] chose the following unitary sequence on the scalar field, Eq. (2):

NLS: $\left|\psi(t+\Delta t)\right\rangle = S_2^T CS_2.C.S_2^T CS_2.C.e^{-i\varepsilon^2 V/2} \, S_1^T CS_1.C.S_1^T CS_1.C.e^{-i\varepsilon^2 V/2}\left|\psi(t)\right\rangle$ (4)

where we choose $V = |\psi|^2 = |\alpha+\beta|^2$. The unitary collision operator C is the $\sqrt{SWAP}$ gate:

$$C = \frac{1}{2}\begin{pmatrix} 1-i & 1\_i \\ 1+i & 1-I \end{pmatrix} \quad \text{with} \quad C^2\begin{pmatrix} \alpha \\ \beta \end{pmatrix} = \begin{pmatrix} \beta \\ \alpha \end{pmatrix} \text{ and } C^4 = I, \tag{5}$$

so-called since C^2 swaps the amplitudes $\alpha \square \beta$. S_1 is the unitary streaming operator shifting the probability amplitude α from lattice site $x \to x + \Delta x$ while transpose $S_1^T : x \to x - \Delta x$. S_2 acts on amplitude β. The QLG algorithm (4) recovers the 1D NLS (3) under the moments $\psi \equiv \alpha + \beta$, with parabolic ordering $\Delta t = \Delta x^2 = \varepsilon^2$. The method is explicit and 2nd order accurate. Numerically, we [5] find that this $\sqrt{SWAP}$ unitary algorithm only recovers the analytic NLS soliton provided the scalar function $|\psi|_{max} \le 0.03$ - which essentially bounds the theoretical ε. QLG algorithms have also been developed for 1D KdV equation [5] and for 1D MHD turbulence [7].

Because of its extreme importance in all branches of physics (from climate modeling to fusion plasmas), classical turbulence continues to be intensively studied now for over 100 years [8]. Turbulence in superfluids has also been strongly pursued for over 50 years [9]. Originally a two-fluid model was introduced (normal and superfluid components) [10], with Feynman [11] suggesting that the superfluid component could rotate if there were quantized vortex lines present. He defined quantum turbulence as the occurrence of strongly tangled vortex lines. When cold atom BECs were obtained experimentally [12, 13], quantum superfluidity could now be studied without any normal fluid component: the condensate wave function satisfies the GP equation

$$i\frac{\partial \psi(\mathbf{x},t)}{\partial t} = \left[-\nabla^2 - \mu + g|\psi(\mathbf{x},t)|^2 \right] \psi(\mathbf{x},t) \tag{6}$$

where μ is the chemical potential, and the nonlinear term $g|\psi|^2 \psi$ arises from the weak s-wave Boson interactions. The GP Eq. (6) is nothing but a 3D NLS equation of nonlinear optics. The quantum turbulence regime is not achievable experimentally, even in the foreseeable future, but can be studied by our QLG algorithm on supercomputers because of its ideal parallelization. Interestingly, the GP equation is Hamiltonian and can be written in fluid-like density and mean velocity variables $(\rho, \mathbf{u}_s)$ by introducing the Madelung transformation

$$\psi(\mathbf{x},t) = \sqrt{\rho(\mathbf{x},t)} \exp\left[i\varphi(\mathbf{x},t) \right] \quad , \quad \mathbf{u}_s(\mathbf{x},t) = \nabla\varphi(\mathbf{x},t) \quad . \quad . \tag{7}$$

Indeed, under this transformation the GP Eq. (6) yield the closed set of hydrodynamic equations

$$\frac{\partial \rho}{\partial t} + \nabla\cdot(\rho\mathbf{u}_s) = 0 \quad and \quad \rho\left(\frac{\partial}{\partial t}+\mathbf{u}_s\cdot\nabla\right)\mathbf{u}_s = -\nabla p \ + \ \nabla\cdot\vec{\Sigma} \tag{8}$$

where the barotropic pressure $p \sim g\rho^2$, and the so-called quantum stress tensor Σ_{ij}:

$$\Sigma_{ij} = \rho\frac{\partial^2 \ln\rho}{\partial x_i \partial x_j} \tag{9}$$

Thus the dynamics of the BEC ground state, under the mean field approximation, is described by a *compressible*, inviscid Euler-like superfluid (i.e., no viscosity) with a novel quantum stress, Eq. (9). It is this quantum stress term that yields the somewhat startling differences between quantum turbulence (QT) and classical (incompressible) Navier-Stokes turbulence (CT): in CT, vortex reconnection can only occur in the presence of viscosity, but quantum vortex reconnection [14] proceeds without any viscosity. Moreover, the vortex is a well defined structure in QT: the wave function ψ is an order parameter for the scalar GP Eq. (6), with the quantum vortex core being a topological singularity $\psi = 0 = \rho$. In CT, however, a classical vortex is a murky concept. By rotating a trapped BEC, the experimentalists [15] were able to create a lattice of quantum vortices – each vortex having the same quantized (discrete) strength (*n* integer), Fig. 1

$$\oint \mathbf{u}_s \cdot d\ell = n\kappa \tag{10}$$

On the other hand, classical vortices/eddies have a continuous range of circulation, and can exist in incompressible fluids (unlike scalar quantum vortices that fundamentally require compressibility for their existence).
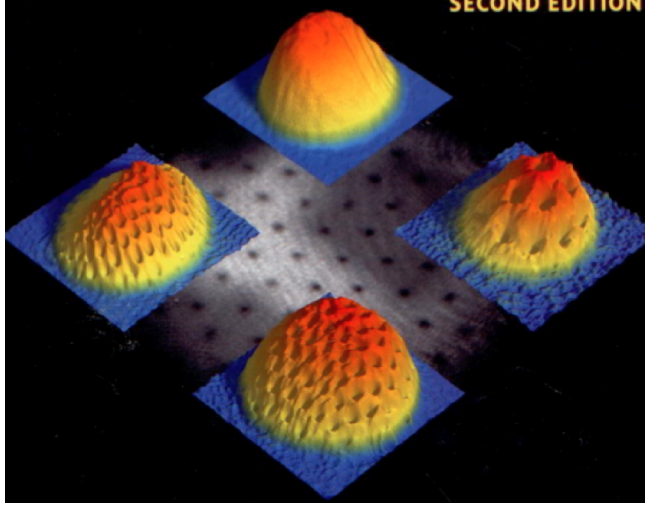
Fig. 1 The formation of a quantum vortex lattice in a rotating BEC. The quantum vortex can be readily identified by the zero density at the quantum vortex core, which in these plots of the BEC density show up as cavities: at the top, the BEC rotation is too low for the existence of a quantum vortex. Moving clockwise, one finds 16 quantum cores, then 70 quantum cores and finally 130 quantum cores (from Ketterle et. al [15]) as the BEC is rotated more rapidly.

One of the most celebrated results of 3D incompressible CT is the Kolmogorov $k^{-5/3}$ energy spectrum in the inertial range [16, 17] as energy is transferred from large to smaller and even smaller vortices till gobbled up viscosity. There has been much work performed in examining the corresponding cascades and energy spectra in QT - with much continuing vigorous dispute [18] and into which we [19] also joined the fray because our QLG code could perform production runs on 5760³ grid without the addition of artificial numerical dissipation. [The largest production DNS simulations of CT that we are aware of is just 4096³]. We achieved these grids because of the extreme parallelization and low memory demands from the 2 qubits/lattice site for 3D simulations. Only 12,288 cores on a CRAY XT-5 were utilized.

That the quantum vortices are topological singularities is readily seen in the evolution of the
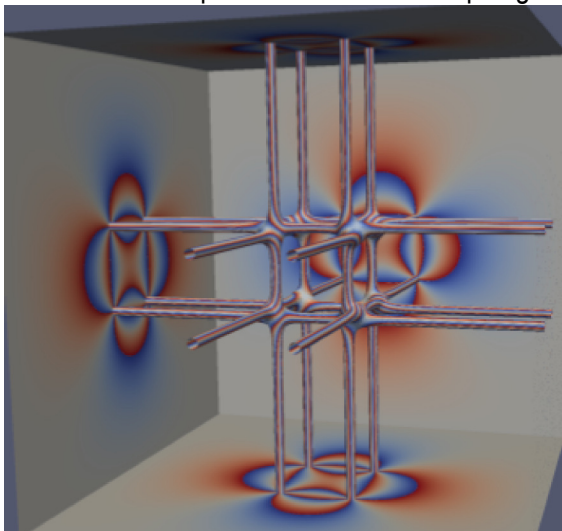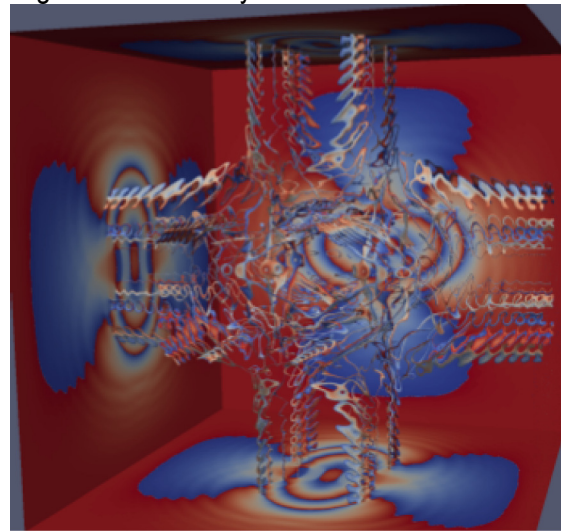
(a) t = 0   (b) t = 3000

Fig. 2 The splitting of the 5-fold degenerate quantum vortices at t = 0 into 5 non-degenerate vortices, (b). Lattice grid 2048^3. Phase information on both the cores and the walls : $\varphi = 0$ (blue), $\varphi = 2\pi$ (red). The oscillations on the cores are Kelvin waves.
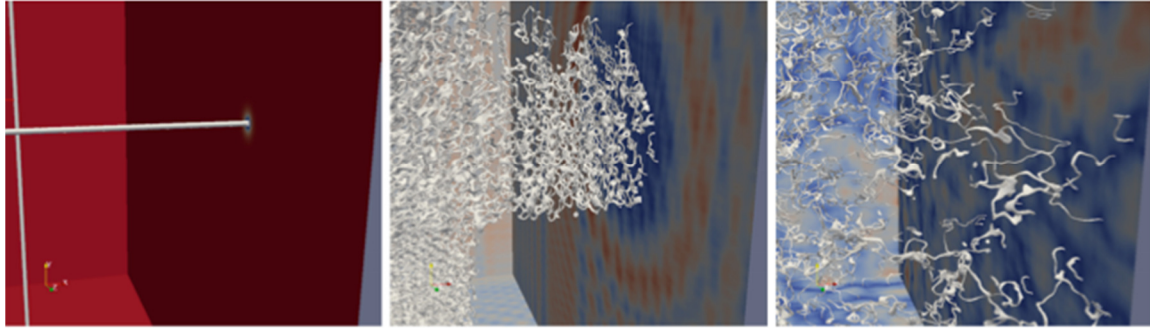
isosurfaces of initial straight line vortex cores with high winding-number-5: $\psi = \sqrt{\rho}\, e^{5i\varphi}$, Fig. 2. The vortex core $(\rho = 0)$ topological singularity appears as a branch-point like singularity – here there will be 5 branch cuts connecting each core as, readily seen at its intercept with the walls. Very rapidly these cores change to the energetically more favorable winding-number-1 cores, with the excitation of (Kelvin) waves along the cores.

2. SOME QLG SIMULATIONS RESULTS ON QUANTUM TURBULENCE
(a) Scalar QT in 3D and 2D

We wish to illustrate some of the results obtained with the $\sqrt{SWAP}$ -unitary collision operator algorithm, even though only small amplitudes can be handled. Later in this proposal we will describe our new Dirac-induced QLG unitary algorithm [20] that permits simulations with amplitudes a factor of 20 greater than with the older algorithm and so permit study of spinor BECs.

The rapid development of tangled quantum vortices in QLG simulation of scalar QT from an initial set of line vortices is shown in Fig. 3. These isosurfaces were generated using *PARAVIEW*, using bit-griding of the phase and magnitude of the wave function at each grid point.

(a)   t = 0   (b) t = 400   (c) t = 57 500

Fig. 3 A zoomed-in section of the GP time evolution of the isosurfaces of 2 quantum line vortex cores (from a total of 12 such vortices) on a spatial grid of 4032^3. (a) At t = 0 , the vortex core isosurfaces for initial winding number 6 – which is very unstable. By t = 400, (b), the cores have expanded and fragmented into n = 1 vortices with entanglement. (c) Vortex tangle is evident at time t = 57 500. Wall color scheme: $|\psi|_{max} - red$, $|\psi|_{min} - blue$.. No phase information is shown on these cores (and hence their white color). Graphics generation/time instant : 120 secs to process 4032^3 data points with 512 cores on a CRAY XE6.

Currently a much more refined visualization package is now being installed in coordination with some computer scientists at DoD's PETTT (Production Enhancement, Technology, Transfer and Training) which automatically generates the ,png files with scaling tested to 150K cores.

We have computed the spectrum of 3D scalar BEC quantum turbulence on a grid of 5760^3 - a topic of considerable interest in the cold atom/He^3 community. The total kinetic energy spectrum (including both compressible and incompressible energies) is shown in Fig. 4. It should be noted that the spectra exponents are not necessarily that rugged, but can be dependent on the chosen wave number band. For example one can find a Kolmogorov-like energy spectrum of $k^{-5/3}$ in the small wave number band $100 < k < 200$, but the exponent shifts to $k^{-4/3}$ in the band $30 < k < 200$. The 3 distinct spectral regions are indicative of multi-scale physics.
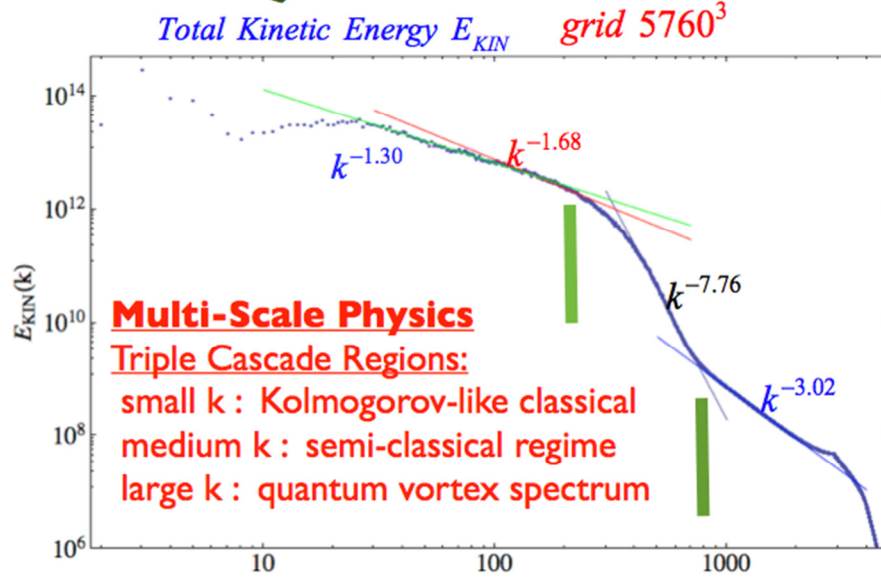
Fig. 4 The total kinetic energy spectrum $E_{kin}(k)$ from a 5760^3 grid simulation. There are 3 clear power law spectral exponents: For large k (800 < k < 2500) $E_{kin}(k) \approx k^{-3}$, for intermediate k (300 < k < 700) a steep $E_{kin}(k) \approx k^{-7.8}$, while for small k (100 < k < 200) $E_{kin}(k) \approx k^{-5.3}$.

Detailed 3D spectra for compressible, incompressible and quantum (related to $\nabla\sqrt{\rho}$) kinetic energies) are shown in Fig. 5 for a 3072^3 run at t = 0 and after 48K time steps. The *incompressible* kinetic energy (blue curve) does not exhibit a Kolmogorov-like spectrum, but a power law that varies from -2.72 for small k to -3.01 for large k. The *total* kinetic energy exponent is -1.66 for small k.
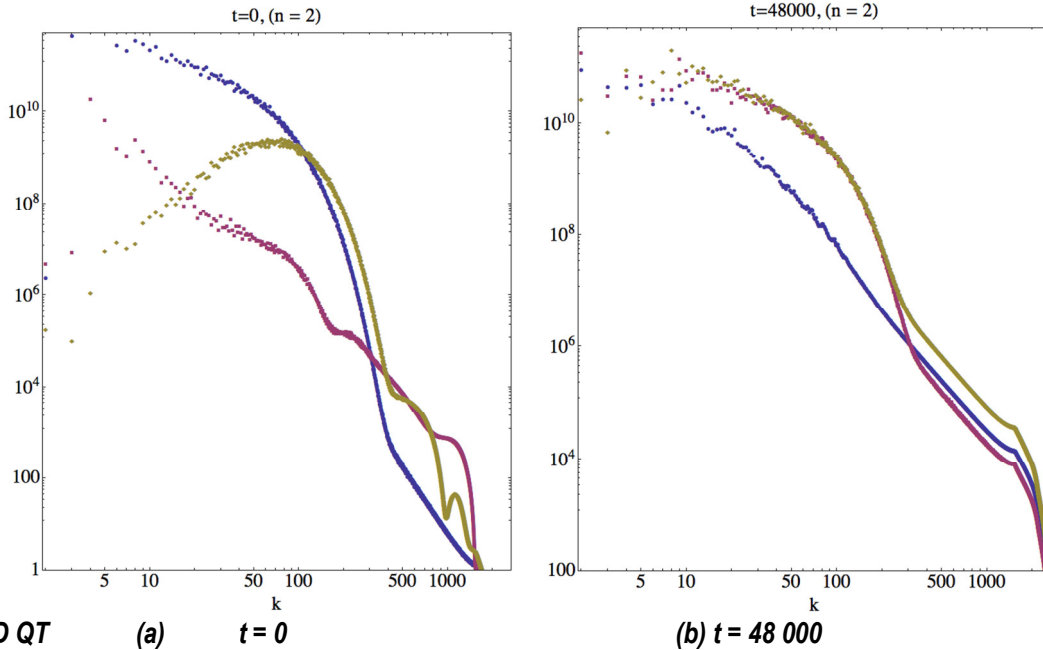

Fig. 5 Spectra for n-2 winding number vortices at (a) t = 0, and (b) t = 48 000 on 3072^3 grid
Color Scheme: blue – incompressible KE, red – compressible KE, gold – quantum energy

One can ask a fundmental question: What are the spectral properties of 2D QT? Are they similar to that for 3D QT? In CT, there is a fundamental difference between 2D and 3D turbulent cascades: in 2D energy inverse cascades to small k, while in 3D energy cascades to large k. Earlier, some researchers [22, 23] have performed CFD-like simulations that indicated that 2D and 3D QT are similar (as, e.g., in 2D and 3D MHD turbulence). In CT, this difference in spectral properties between 2D and 3D is attributed to the existence in 2D of a new quadratic invariant – the mean square vorticity. There is no such similar invariant in 2D QT. With our QLG algorithm [25], we also find similarity between 2D and 3D QT spectra – here the 2D QT simulations were on 8192^2 grid – as can be seen by comparing Figs. 5 & 6. Thus benchmarking our QLG algorithm with more standard CFD algorithms.
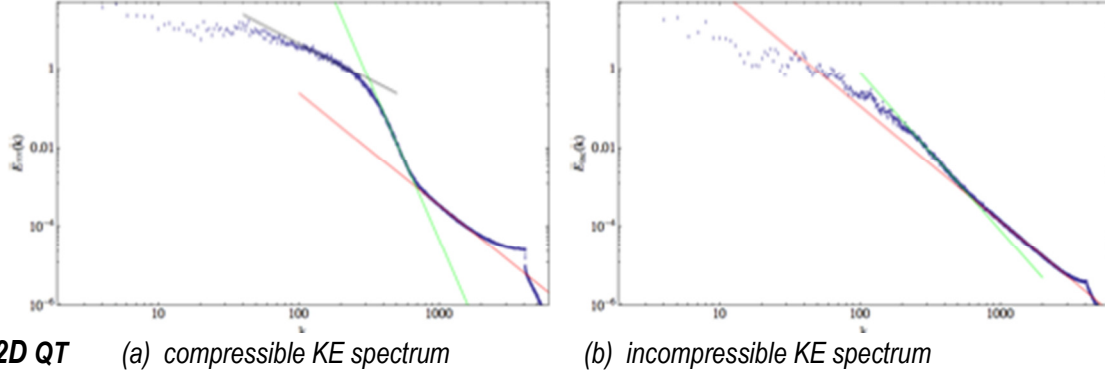
2D QT   *(a) compressible KE spectrum*   *(b) incompressible KE spectrum*

*Fig. 6 (a) For the **compressible** kinetic energy spectrum, there are again 3 distinct power law spectral regions $k^{-\alpha}$: $\alpha = 1.83$ (small k, black), $\alpha = 8.1$ (intermediate k, green), and $\alpha = 2.85$ (large k, red). (b) For the **incompressible** KE spectrum, $\alpha = 2.93$ (large k, red) and $\alpha = 4.00$ (intermediate k, green).*

(b) Coupled BECs – coreless vortices

Our $\sqrt{SWAP}$ - QLG algorithm is readily extended [26] to solve a system of coupled BECs with their different topological vortex structure. In particular, skyrmions are topological defects in a continuous field which are spatially localized with a quantized topological charge that can undergo interactions and phase transitions. Because of these topological properties, skyrmions were actually first introduced into baryon elementary particle physics [27], and have since been applied to studies in liquid crystals [28], BECs [29] and quantum Hall effects [30, 31]. Moreover, they can exhibit vortex lattice structures not unlike type II superconductors [32]. The evolution of the skyrmion Ψ in coupled BECs is governed by the coupled GP equation, requiring just 4 qubits/lattice grid point in our QLG algorithm:

$$i\frac{\partial \Psi}{\partial t} = -\nabla^2 \Psi + a\left[g\left(\left\{\left|\psi_+\right|^2 + \left|\psi_-\right|^2\right\} - 1\right) \right]\Psi \quad , \quad with \quad \Psi = \begin{pmatrix} \psi_+ \\ \psi_- \end{pmatrix} \rightarrow \begin{pmatrix} 0 \\ 1 \end{pmatrix} \quad as \quad \left|\mathbf{x}\right| \rightarrow \infty \tag{11}$$

The skyrmion spinor is a coreless vortex with vortex core components as shown in Fig. 7 : a vortex ring (component $\left|\psi_+\right| \sim 0$, in green) linked by a linear vortex core threading through the ring center and closing at infinity (component $\left|\psi_-\right| \sim 0$, in orange). This linear vortex core component is analogous to the 1D scalar vortex core discussed earlier. The skyrmion is a coreless vortex since Ψ is never a zero spinor. By varying its amplitude, the skyrmion is no longer a stable solution of the nonlinear Eq. (11) and the core isosurface expands. On interacting with the walls, it forms a percolating lattice of vortex rings forming capulae on many but not all of the lattice structure defects, Fig. 8. Since the filling fraction of the vortex ring condensate $\left(\left|\psi_+\right|\right)$ is too low

to support quantum vortex rings on all the quantum vortex nodal lines of $|\psi_-|$ in the lattice, the $|\psi_+|$ condensate appears to randomly percolate throughout the lattice of the $|\psi_-|$ condensate.
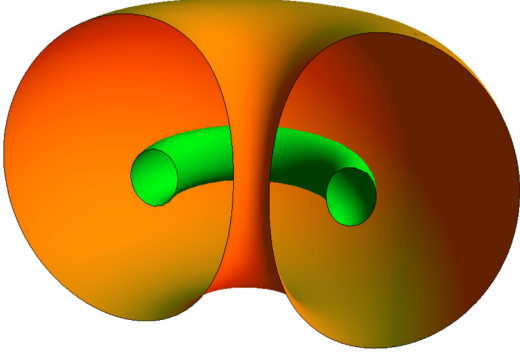

Fig. 7 Coreless vortex in a spinor BEC : a vortex ring (green) threaded by a linear vortex that then closes at infinity (orange) on itself. Grid 1024^3.
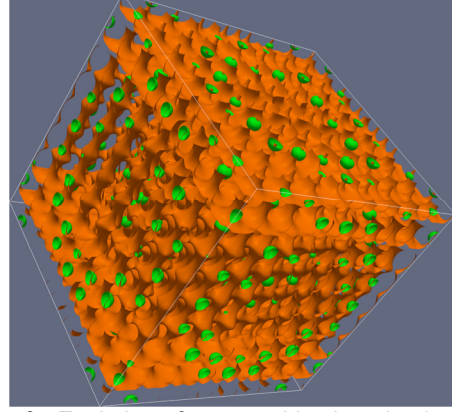

Fig. 8   Evolution of an unstable skyrmion into a percolating lattice structure of skyrmion-like defects. The vortex ring cores (green) now form capulae and (when present) are threaded by the linear vortex cores.

3. CUURENT RESEARCH

A major problem of interest is considering spinor QT involving non-Abelian vortices. In particular, could non-Abelian structures play as an important and fundamental role in QT as non-Abelian gauge theory have played in bridging the Abelian gauge theory of quantum electrodynamics to now be able to include strong interactions in high energy physics?

Now BECs trapped in magnetic wells have their spin aligned with the magnetic field, resulting in a scalar topological charge and Abelian quantum vortices. The dynamics of such BECs is well described in the mean field approximation by the scalar GP Eq. (6) and is still a most active area of research together with coupled BECs and the instabilities that can arise (e. g., quantum Kelvin-Helmholtz instability [33, 34]). However, in optical traps the spin orientation can dynamically precess giving rise to spin degrees of freedom which will require a spinor GP representation of the ground state dynamics. Now the spinor vortex can have much more complex structure than the simple scalar vortex. For example, we can now have "coreless" vortices which, like skyrmions, can have some components of the order parameter that are non-zero at the spinor vortex core. For spin-1 BECs (like ^{23}Na or ^{87}Rb), the mean field dynamics are given by [35]

$$i\frac{\partial \psi_m}{\partial t} = -\left(\nabla - U_{trap}\right)\psi_m + a\left[g\sum_{k=-1}^{1}|\psi_k|^2\right]\psi_m + b\sum_{k=-1}^{1}\mathbf{F}\Box \mathbf{f}_{mk}\,\psi_k \quad , \quad m=-1,0,1 \qquad (12)$$

where U_{trap} is the trapping potential, $\mathbf{F}$ the spin density vector, and $\mathbf{f}$ the usual spin-1 matrices :

$$F_\alpha = \sum_{m,k=-1}^{1} \psi_m^*(\mathbf{x})[f_\alpha]_{mk}\,\psi_k(\mathbf{x}) \quad , \quad \alpha=x,y,z$$

$$\qquad (13)$$

However the $\sqrt{SWAP}$-QLG algorithm, which requires small amplitude wave functions, could not adequately simulate the spin-1 BECs. We are thus now examining a recent QLG devised by

Yepez [20] for the solution of the 1D Dirac equation. First, in the non-relativistic limit, we extend the algorithm to solve the 1D NLS/GP Eq. (3). In this QLGD algorithm, the unitary collision is

$$C_D = \begin{pmatrix} \cos\left[\pi/4+\varepsilon^2 V\right] & -i\sin\left[\pi/4+\varepsilon^2 V\right] \\ -i\sin\left[\pi/4+\varepsilon^2 V\right] & \cos\left[\pi/4+\varepsilon^2 V\right] \end{pmatrix}, \quad \text{with} \quad V(x) = -|\psi|^2 \qquad (14)$$

with the QLGD sequence of interleaved unitary collide-stream operators [c.f., with Eq. (4)]

NLS: $\left|\psi(t+\Delta t)\right\rangle = S_2^T C_D S_2 C_D . S_2^T C_D S_2 C_D . \ S_1^T C_D S_1 C_D . S_1^T C_D S_1 C_D \left|\psi(t)\right\rangle$ \qquad (4')

Applied to the 1D NLS soliton collision problem, this new QLGD algorithm reproduced the exact theoretical soliton physics and soliton collision-induced shifts, but at amplitudes a factor of over 20 greater than with the old $\sqrt{SWAP}$ -collision operator, $\left|\psi_{max}\right|_{QLGD} \leq 0.6$, and with soliton speeds over a factor of 5 greater. This is a critical finding as it permits a much larger ε than before.

We have just now performed some exploratory runs on the spin-1 spinor BECs and find that our QLGD algorithm, for the first time, can handle this problem. In essence, there are 2 major constants of the motion of our unitary algorithm: the mean density and the total energy of the Hamiltonian system. A violation of the total energy is an immediate indicator that our initial conditions (on the wave function amplitudes) are not appropriate. Our QLG/D algorithms are perturbative in ε in the sense that we recover asymptotically the spin-1 GP system, Eq. (12), whose total energy is a constant of the motion (and identifying its various terms):

$$\underset{\text{kinetic}}{} \quad \underset{\text{potential}}{} \quad \underset{\text{spin-indep. s-wave}}{} \quad \underset{\text{new spin-dep. Interaction}}{}$$

$$E_{TOT} = \int d^3 x \left[\sum_{m=-1}^{1}\left\{ \left|\nabla\psi_m\right|^2 + U_{pot}\left|\psi_m\right|^2\right\} + \frac{a_0 g}{2}\left(\sum_{m=-1}^{1}\left|\psi_m\right|^2\right)^2 + \frac{b_1}{2}\sum_{\alpha=x,y,z}\left(\sum_{m,n=-1}^{1}\psi_m^*\left[f_\alpha\right]_{mn}\psi_n\right)^2\right]$$

The QLG algorithms, Eqs. (4) and (4'), act on qubits and at this mesosopic level there is no intrinsic energy integral. If in the continuum limit, the QLG recovers the GP equations [to errors of $O(\varepsilon^2)$], then the specific energy integral of the GP system must be conserved by the QLG model. If we are in a parameter regime in which the QLG model does not recover the continuum GP equations, then the computation of E_{TOT} from the qubits will not be conserved.
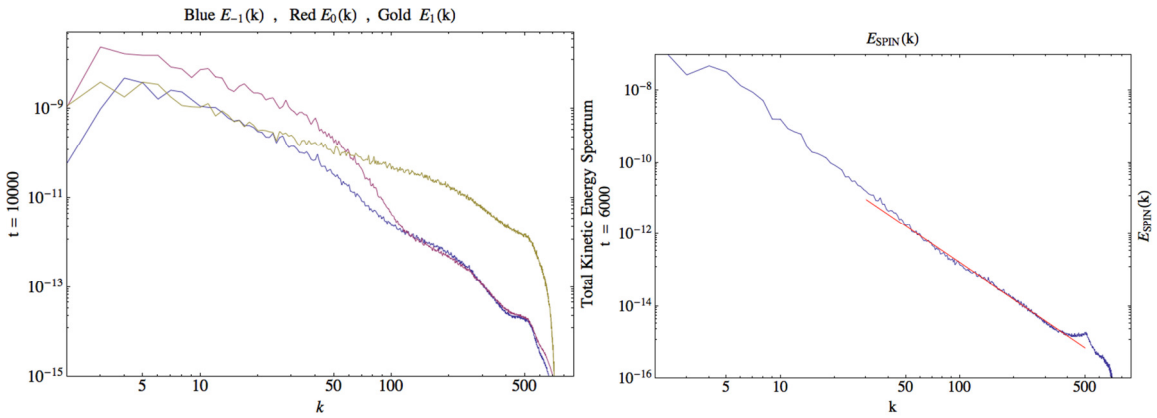
(a) *total kinetic energy spectra* (b) *spin energy interaction spectrum*

Fig. 9 *(a) The total kinetic energy spectrum for the spin-1 BEC components : m = -1, 0 and 1. The m = +1 energy spectrum is somewhat different from the other m's, exhibiting a -4/3 spectral exponent; (b) The spin*
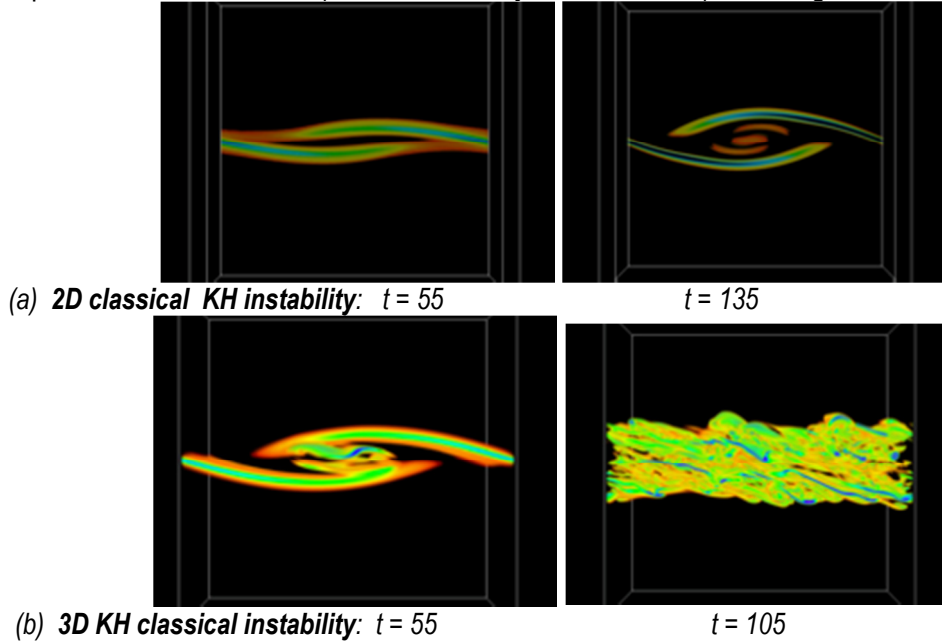
energy spectrum exhibiting a -10/3 spectum in the early stages (t = 10000) of 3D spinor turbulence on 1024³ grid. In 2D spinor turbulence, Tsubota et. al. claim a -7/3 spectral exponent [36] . We obtained these initial results in the middle of June, 2014. More extended runs will be performed with different initial conditions to test the universality of the spectra.

We now outline some of the production runs we are planning

(a) quantum Kelvin-Helmholtz instability in 2D and 3D

The classical KH instability is ubiquitous and arises in strong velocity shear within a fluid or a velocity shear layer between two different fluids. It occurs in plasmas, the oceans, the atmosphere, Saturn bands, Jupiter's red spot as well as in the sun's corona. Roll-up vortices of opposite circulation on either side of the shear interface occur with the formation of billow structures. For sufficiently high Reynolds numbers, these vortices continue to strengthen until they eventually disrupt the shear interface and lead to general 2D turbulence: merging of like-signed vortices into larger vortices, forming larger and larger vortices due to the inverse cascade of 2D CT. 3D KH is substantially different due to, presumably, the direct cascade of energy to small scales and due to the fact that the vorticity vector is no longer restricted in the direction perpendicular to the motion (a 'scalar' vorticity direction in 2D) – see Fig. 10

(a) **2D classical KH instability**: *t = 55*   *t = 135*

(b) **3D KH classical instability**: *t = 55*   *t = 105*

Fig. 10 *Effect of dimensionality -: (a) 2D, (b) 3D – for the y-component of vorticity in classical KH instability -- from Skillman et. al. [37]. Re = 2300 , Richardson number = 0.2*

Only 2D quantum KH instability has so far been investigated experimentally [37] and theoretically in [38], with the typical development of a sawtooth interface and then the shedding of quantized vortices of the same strength from the peaks of the sawteeth. This leads to a decrease in the relative shear across the interface between the two immiscible BECs and no further vortex nucleation occurs. Takeuchi et. al. [38] solve the coupled BEC system, basically Eq. (11) using standard CFD algorithms (with numerical dissipation added to stabilitize the simulation) – Fig. 11.

We propose to study the quantum KH instability in both 2D and 3D using our QLGD BEC2-code. Very high resolution runs can now be performed because of the parallelization of our algorithm. We will also be in a position to study the differences between 2D and 3D KH-induced

turbulence. Moreover, because of the extreme parallelizability of the QLGD-codes we can run sufficiently large grids (parallelization tested to grids 9600^3) to study how spatial averaged regions can bridge and explain the difference between 2D and 3D classical physics. This has not yet been satisfactorily achieved to date.
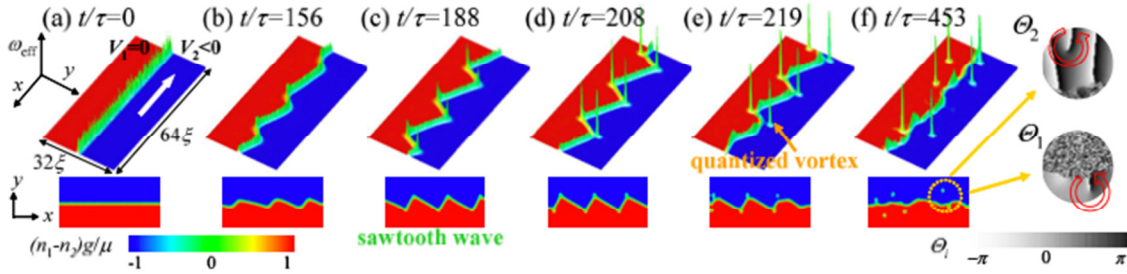

Fig. 11 The 2D quantum KH instability between two immiscible BECs with velocity shear at different times. Upper panels: density-weighted vorticity (with green giving the amplitude of the vorticity, and the $\delta-$functions spikes being the quantized vortices). Lower panels: the mean density of the system. The phases in the Madelung transformation: $\theta_1(y<0), \theta_2(y>0)$ give the rotational direction of these vortices – taken from Takeuchi et. al. [38].

(b) spinor BEC quantum turbulence with non-Abelian vortices

Considerable work has been performed on understanding spinor vortices using homotopy theory [35, 38, 40], but conventional homotopy theory does not reveal much about the structure and dynamics of the spinor vortex cores. A topological classification of vortex-core structures of spinor BECs has been given [40-42] using locally defined winding numbers in the core, and only somewhat recently have some very limited 2D simulations been performed [36] – and these only for s = 1 BECs which support only Abelian vortices. Since the topological charge of a quantum vortex is defined by the change in the corresponding order-parameter as one integrates over a closed path enclosing the core [c.f., Eq. (10)], spinor quantum turbulence will depend critically on the vortex topological charge and the permitted vortex-vortex interactions. For scalar BECs, all the vortices have integer topological charge [*n* integer in Eq. (10)] and are Abelian *U(1)* vortices. However, for spinor BEC, the topological need no longer be integer and there can be classes of vortices that are non-Abelian. Some 2D spinor spin-1 turbulence simulations [45-46] have just been reported which claim the spin-dependent interaction energy obeys a $k^{-7/3}$ power law. However, these simulations also required the introduction of numerical dissipation to stabilize their code. On the other hand, in our unitary QLG algorithms the conservation of energy is fundamental as well as being a most important numerical diagnostic. Morever our unitary algorithms mimic the Hamiltonian structure of the GP equations – thus preserving important intrinsic symmetries.

The effect of non-Abelian vortex-vortex interactions, different topological vortex nucleations … are a massive new area of research in QT in which we feel we can lead the field and make significant contribution based on our unitary QLG algorithms and its parallelization to all available cores on classical supercomputers. Extremely high resolution 3D simulations can now be performed that are not possible using current CFD techniques. In 2D, we expect to achieve a much longer power law k-range. We are collaborating with computer scientists in i/o and co-processing visualization data to be able to handle hundreds of TB data efficiently, rapidly and on the fly. Moreover, our QLG algorithm – because of the unitarity of the qubit collision-stream operators – is readily encoded onto quantum computers when available. Another important feature

of our QLG codes are their very low memory requirements: to simulate 3D spin-1 BECs we only require 6 qubits/lattice site (2 qubits for each $\psi_m, m = -1,0,1$); for 3D spin-2 BECs we will need 10 qubits/lattice site to solve the 5 coupled GP equations.

## 4. PARALLEL PERFORMANCE OF QLG ALGORITHMS ON THE IBM/BLUEGENE Q *MIRA*

We now consider the scaling of our SPIN1-code [for spinor BEC, Eq. (16)] and the BEC2-code [for coupled BECs, Eq. (15)] . In strong scaling, the grid is held fixed while the number of cores is increased leading to corresponding reduction in wall clock time. In weak scaling, the work performed on each core is held fixed by increasing the grid and number of cores proportionally.

Table 1. Strong Scaling: Grid 9600^3 to the full 48 racks on IBM/BG Q (Mira)

#nodes	Ranks – Mode C32	Time (s)	Speed-up [ideal]
16 384	524 288	816.1	1.0 [1.0]
32 768	1 048 576	389.7	2.1 [2.0]
49 152	1 572 864	275.8	3.0 [3.0]

Fig. 12 Strong scaling of spinor BEC algorithm on Mira, using 2 MPI ranks/core with 16 cores/node (blue curve). The red dashed curve is ideal scaling up to the full 786 432 cores available on Mira. The multiple MPI ranks/core gives the benefit of multiple instruction issue by multiple threads on the BG/Q chip while running the code in pure MPI mode.
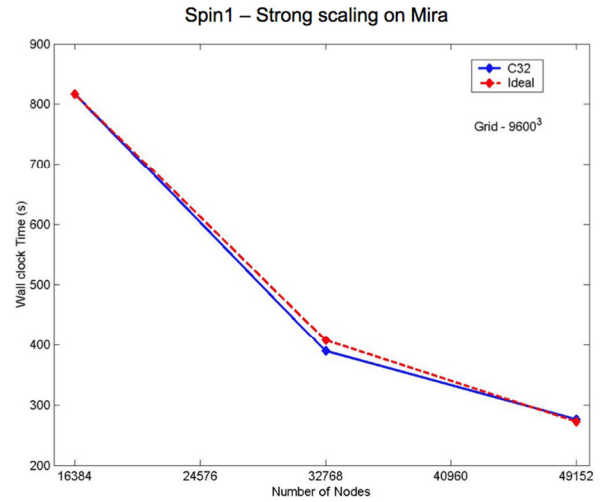
Note that our QLG codes place a very low memory requirement on the cores, even for 3D simulations since each scalar order parameter wave function requires only 2 qubits/lattice site. The 3D aspects of the problem are handled by the sequence of unitary collision/stream operators.

As seen in Table 1 and Fig. 12, the SPIN1-code has excellent strong scaling on the IBM/BG Q. These runs were performed with –mode c32, i.e., with 2 MPI ranks/core. This gives the benefit of dual instruction issue by 2 threads on the BG/Q chip while running the code in pure MPI mode.

The weak scaling of the SPIN1-code was tested up to 262,144 cores (16 racks) using (a) 1 MPI rank/core (mode c16), and (b) 4 MPI ranks/core (mode c64), Table 2. The wallclock time is quite flat, with less than 4% variation form the mean.

Table 2. Weak Scaling: Spin1- code on IBM/BlueGeneQ (Mira) : 50 iterations

(a)   1 MPI rank/core

Grid	Nodes	Ranks – Mode C16	Time (s)
800^3	32	512	323.4
1600^3	256	4096	323.4
3200^3	2048	32 768	323.7
6400^3	16 384	262 144	326.5

(b)   4 MPI ranks/core

Grid	Nodes	Ranks – Mode C64	Time (s)
800^3	32	2048	203.7
1600^3	256	16 384	197.1
3200^3	2048	131 072	197.8
6400^3	16 384	1 048 576	209.6

For a fixed number of cores, there is significant speed-up in using multiple MPI ranks/core for the BEC2-code on *MIRA*, Table 3. Of course, as one increases the number of ranks/core the amount of memory available for each process is reduced.

Table 3 (a) scaling with MPI ranks: BEC2-code. (100 iterations) – 1 rack, 2048^3 grid

Ranks	#MPI ranks /core	Time (s)	Speed -up
16 384	1	265.3	1
32 768	2	181.1	1.46
65 536	4	158.5	1.68

(b) MIRA scaling with MPI ranks: BEC2-code (50 iterations) – 8 racks, 5120^3 grid

Ranks	#MPI ranks /core	Time (s)	Speed -up
131 072	1	246.7	1
262 144	2	183.1	1.35
524 288	4	155.7	1.59

OpenMP Timings

With significant help from ALCF staff we have converted our Spin1-code to a hybrid MPI/OpenMP code using OpenMP loop parallelization directives. The timings in Tables 4 and 5 show good 'strong scaling' in this hybrid mode, using 16 MPI ranks/node (1 rank/core) and 4 OpenMP threads. The parallel efficiency had only reduced to 94.1% on 32 racks, achieving 1.174 PFlops. There is a very high percentage of L1 cache hits in our memory references, with quite low main memory (DDR) hits.

Table 4.   Strong Scaling , OpenMP Timings,   Grid 5120^3 - to 32 racks

	4 racks	8 racks	16 racks	32 racks
Wallclock (s)	406.11	203.62	106.58	53.94
Cores	65 536	131 072	262 144	524 288
Parallel efficiency	100%	99.7%	95.3%	94.1%
L1 d-cache	88.64%	89.13%	89.11%	88.79%
DDR	2.59%	2.51%	2.56%	2.63%
GFlops/node	38.42	38.35	36.34	36.12
PFlops	0.156	0.311	0.595	1.174

In Table 5, we see similar excellent strong scaling using the same mode (C16-mode with OMP_NUM_THREADS=4), for 2560^3 grid runs up to 8 racks.

Table 5.   Strong Scaling , OpenMP Timings,   Grid 2560^3 - to 8 racks

	0.5 racks	1 rack	2 racks	4 racks	8 racks
Wallclock (s)	406.11	203.38	106.53	53.67	27.21
Cores	8 192	16 384	32 768	65 536	131 072
Parallel efficiency	100%	99.8%	95.3%	94.6%	93.3%
L1 d-cache	88.38%	88.43%	88.98%	88.90%	89.10%
DDR	2.65%	2.64%	2.59%	2.61%	2.65%
GFlops/node	38.24	38.14	36.44	36.12	33.72

I/O Performance

With help from ALCF i/o staff, we have implemented restart i/o by GLEAN. Timings shown in Table 6 are for the SPIN1 code (6 double complex arrays; 2 for each wave function are dumped) by 16 MPI ranks/node.

Our 3D proposed runs are going to evolve 100K time steps on 5120^3 grids with restart dumps of 35TBs. I/O dumps for spectral analysis are going to be performed every 5K time steps;

but will require only single precision wave functions. Thus time for i/o dumps are going to be less than 0.5% of the wall clock needed for 5K time steps.

Table 6   I/O Performance by GLEAN.

Actual wallclock time between outputs: 32,000 s (for the 1st and 3rd rows)

Grid	Nodes	Ranks	I/O Time [s]	Throughput [GB/s]
3200^3	2,048	32,768	190.2 s	15.4
3200^3	8,192	131,072	65.4 s	44.8
6400^3	16,384	262,144	241.2 s	97.2
6400^3	32,767	524,288	170.6 s	137.4

ADIOS I/O on Mira: Throughputs we are now getting with ADIOS I/O are also similarly high. The #s below in Table 7 are for SPIN1-code restart i/o with a new method for BGQ. [Since the data can be read back straight (using arbitrary cores) into any shape with the needed ghost cells, we are now using this for the analysis i/o as well]. Note: No Meta data files are here written out separate like the way we do earlier with our previous version on other platforms. They are instead distributed on all files in each directory.

Table 7. ADIOS I/O on Mira GPFS

Grid	Nodes	Ranks	I/O Time [s]	Throughput [GB/s]
6400^3	16384	262,144	193	121.4
6400^3	32767	524,288	183	128.1

N.B: These timings are with the $\sqrt{SWAP}$ -collision operator. Our new QLGD algorithm utilizes a similar unitary collide-stream operator sequence but with a more intricate collision operator C_D, Eq. (14). Since C_D is still purely local, the parallelization will not be affected but it will add at least 20% extra to the wallclock time.

Visualization i/o

To generate the vortex isosurfaces shown in Figs. 2, 3 and 8, the traditional (POSIX) i/o system was modified to limit the number of parallel tasks that simultaneously access the file system at once. This reduces the load on the metadata server employed by the parallel file systems and solves one of the most common parallel i/o bottlenecks. Each task of the code writes to a separate file and to minimize directory entry overload, files are grouped into subdirectories. The current visualization i/o being developed will be built onto the MPI or *Adios* i/o. Co-processing of data will be accomplished with the open source software *PARAVIEW* throughout the run. This will permit *in situ* visualization and feature extraction and eliminate the need for nearly all disk i/o (except that needed for spectral analysis).

REFERENCES
[1] M. A. Nielsen and I. L. Chuang, *Quantum Computation and Quantum Information* (Cambridge Univ. Press, 2010 Ed.), T. Byrnes, K. Wen and Y. Yamamoto, Phys> Rev. **A85**, 040306(R) (2012).
[2] E. P. Gross, J. Math. Phys. **4**, 195 (1963); V. L. Ginsburg and L. P. Pitaevskii, J. Phys. USSR **7**, 858 (1958)
[3] J. Yepez, Intl. J. Mod. Phys. **C9**, 1587 (1998); J. Yepez, Phys. Rev. **E63**, 046702 (2001); J. Yepez and B. Boghosian, Comput. Phys. Commun. **146**, 280 (2002); D. A. Meyer, Philos. Trans. R. Soc. London. Sect **A360**, 395 (2002); D. A. Meyer, Philos. Trans. R. Soc. London. Sect **A360**, 395 (2002); S. Succi, Intl. J.

Mod. Phys. **C9**, 1577 (1998

[4] K. Fujimoto and M. Tsubota, Phys. Rev. **A85**, 053641 (2012); Phys. Rev. **A85**, 033642 (2012); M. Tsubota, Y. Aoki and K. Fujimoto, arXiv:1304.4674 (2013).

[5] G. Vahala, J. Yepez, and L. Vahala, Phys. Lett. **A310**, 187 (2003)

[6] G. Vahala, L. Vahala and J. Yepez, Phil. Trans. Roy. Soc. London, **362**, 1677 (2004).

[7] L. Vahala, G. Vahala and J. Yepez, Phys. Lett. **A306**, 227 (2003); J. Fleischer and P. H. Diamond, Phys. Rev. E61, R2709 (1998); Phys. Rev. E61, 3912 (2000)

[8] S. B. Pope, *Turbulent Flows* (Cambridge University Press, New York, 1990).

[9] W. F. Vinen, J. Low Temp. Phys. **145**, 7 (2006)

[10] F. London, *Superfluids*, Vol. II, Wiley. New York (1954) and references therein; L. Tisza, Nature **141**, 913 (1938); L. D. Landau, J. Phys. Moscow **5**, 71 (1941), **11**, 91 (1947).

[11] R. P. Feynman, Prog. in Low Temp. Phys., vol. I (North-Holland, Amsterdam, 1955

[12] M. H. Anderson, J. R. Ensher, M. R. Matthews, C. E. Wieman and E. A. Cornell, Science **269**, 198 (1995),; K. B. Davis, M. O. Mewes, M. R. Andrews, N. J. van Cruten, D. W. Kurn, and W Ketterle, Phys Rev. Lett. **75**, 3969 (1995).

[13] W. Ketterle and M W. Zwierlein, in *Ultracold Fermi Gases*, ed. M. Ingusio, W. Ketterle and C. Salomon (IOS Press, Amsterdam) 2008

[14] J. Koplik and H. Levine, Phys. Rev. Lett. **71**, 1375 (1993)

[15] J. R. Abo-Shaeer, C. Raman, J. M. Vogels and W. Ketterle, Science **292**, 476 (2001)

[16] A. N. Kolmogorov. C. R. Acad. Sci. URSS **30**, 538 (1941)

[17] H. L. Grant, R. W. Stewart and A. Moillet, J. Fluid Mech. **12**, 241 (1961)

[18] C. F. Barenghi, Physica D **237**, 2195 (2008); A. W. Baggaley and C. F. Barenghi, Phys. Rev. **B83**, 134509 (2011); A. W. Baggaley. C. F. Barenghi, A. Shukurov and Y. A. Sergeev, Europhys. Lett. **98**, 26002 (2012); E. Kozik and B. Svistunov, Phys. Rev. Lett. **92**, 035301 (2004); G. Boffetta, A. Celani, D. Dezzani, J. Laurie and S. Nazarenko, J. Low Temp. Phys. **156**, 193 (2009); V. S. L'vov and S. V. Nazarenko, arXiv:1208.4593 (2012); E. B. Sonin, Phys. Rev. **B85**, 104516 (2012); L. Laurie, V. S. L'vov, S. Nazarenko and O. Rudenko, Phys. Rev. **B81**, 104526 (2010); V. S. L'vov and S. Nazarenko, JETP Lett. **91**, 428 (2010); E. Kozik and B. V. Svistunov, Phys. Rev. **B82**, 140510 (2010); A.W. Baggaley and C. F. Barenghi, Phys. Rev. **B83**, 134509 (2011); V. V. Lebedev, V. S. L'vov and S. V. Nazarenko, J. Low Temp. Phys. **161**, 606 (2010); V. S. L'vov, S. V. Nazarenko and O. Rudenko, Phys. Rev. **B76**, 024520 (2007); G. Krstulovic and M. Brachet, Phys. Rev. Lett. **106**, 115303 (2011); V. S. L'vov, S. V. Nazarenko and O. Rudenko, Phys. Rev. **B76**, 024520 (2007); E, V, Kozik and B. V. Svistunov, J. Low Temp. Phys. **161**, 603 (2010); N. Sasa, T. Kano, M. Machida, V. S. L'vov, O. Rudenko and M. Tsubota, Phys. Rev. **B84**, 54525 (2011); M. Kobayashi and M. Tsubota, Phys. Rev. Lett. **94**, 065302 (2005); M. Tsubota, J. Low Temp. Phys. (to appear 2012); arXiv:1207.3589v1; N. Sasa, T. Kano, M. Machida, V. S. L'vov, O. Rudenko and M. Tsubota, Phys. Rev. **B84**, 54525 (2011); G. P. Bewley, D. P. Lathrop and K. r. Sreenivasan, Nature **441**, 588 (2006); M. S. Paoletti, R. B. Fiorito, K. R. Sreenivasan and D. P. Lathrop, J. Phys. Soc. Japan **77**, 111007 (2008); M S. Paoletti, M. E. Fisher and D. P. Lathrop, Physica **D239**, 1367 (2010); M. Kobayashi and M. Tsubota, Phys. Rev. **A76**, 045603 (2007); E. A. L. Henn, J. A. Seman, G. Roati, K. M. F. Magalhaes and V. S. Bagnato, Phys. Rev. Lett. **103**, 045301 (2009); H. Taakeuchi, S. Ishino and M. Tsubota, Phys. Rev. Lett. **105**, 205301 (2010); S. Ishino, M. Tsubota and H. Takeuchi, Phys. Rev. **A83**, 063602 (2011)

[19] J. Yepez, G. Vahala, L. Vahala and M. Soe, Phys. Rev. Lett. **103**, 084501 (2009), **105**, 129402 (2010)

[20] J. Yepez, *Quantum lattice gas model of Dirac particles in 1+1 dimensions*, arXiv:1307.3595 (2013)

[21] R. H. Kraichnan, Phys. Fluids **10**, 417 (1967) ; G. K. Batchelor, Phys. Fluids **12**, 11 (1969)

[22] T. –L. Horng, C. –H. Hsueh, S. –W. Su, Y. –M. Kao and S. –C. Guo, Phys. Rev. **A80**, 023618 (3009)

[23] R. Numasato, M. Tsubota and V. S. L'vov, Phys. Rev. **A81**, 063630 (2010)

[24] T. W. Neely, E. C. Samson, A. S. Bradley, M. J. Davis and B. P. Anderson, Phys. Rev. Lett. **104**, 160401 (2010); T. W. Neely, A. S. Bradley, E. C. Samson, S. J. Rooney, E. M. Wright, K. J. H. Law, R. Carretero-Gonzalez, P. G. Kevrekidis, M. J. Davis and B. P. Anderson, arXiv:1204.1102v2

[25] B. Zhang, G. Vahala, L. Vahala and M. Soe, Phys. Rev. **E84**, 046701 (2011)

[26] G. Vahala, J. Yepez, L. Vahala and M. Soe, Computat. Sci and Disc. **5**, 014013 (2012)

[27] T. H. Skyrme, Proc. R Soc. Lond. **A260**, 127 (1961)

[28] D. C. Wright and N. D. Mermin, Rev. Mod. Phys. **61**, 385 (1989)

[29] U. Al'Khawaha and H. T. Stoof, Nature **411**, 918 (2001)

[30] S. L. Sondhi, A. Karlhede, S. A. Kivelson and E. H. Rezayi, Phys. Rev. **B47**, 16419 (1993)

[31] L. Brey, A. H. Fertig, R. Cote and A. H. MacDonald, Phys. Rev. Lett. **75**, 2562 (1995)

[32] A. A. Abrikosov, Rev. Mod. Phys. **76**, 975 (2004)

[33] H. Takeuchi, S. Ishino and M. Tsubota, Phys. Rev. Lett. **105**, 205301 (2010)

[34] N. Suzuki, H. Takeuchi, K. Kasamatsu, M. Tsbota and H. Saito, Phys. Rev. **A82**, 063604 (2010)

[35] Y. Kawaguchi and M. Ueda, *Spinor Bose-Einstein condensates* , Physics Reports **520**, 253-381 (Nov. 2012);   M. Ueda, *Fundamentals and New Frontiers of Bose-Einstein Condesnation* (World Sci.Publ., Singapore 2010)

[36] M. Tsubota, Y. Aoki and K. Fujimoto, Phys. Rev. **A88**, 061601 (R) (2013)

[37] S. Skillman, S. Reckinger and S. Reckinger, scales.colorado.edu/reckinger/Pubs/a5_KH.pdfm

[38] H. Takeuchi, N. Suzuki, K. Kasamatsu, H. Saito, and M. Tsubota, Phys. Rev. **B81**, 094517 (2010)

[39] H. Takeuchi, S. Ishino and M. Tsubota, Phys. Rev. Lett. **105**, 205301 (2010)

[40] N. Suzuki, H. Takeuchi, K. Kasamatsu, M. Tsbota and H. Saito, Phys. Rev. **A82**, 063604 (2010)

[41] N. D. Mermin, Rev. Mod. Phys.**51**, 591 (1979)

[42] V. P. Mineev, *Topological stable defects and solitons in ordered media*, Classical Reviews in Physics, vol. 1 (Harwood Academic, Amsterdam, 1998)

[43] G. E. Volovik, *The Universe as a Helium Droplet* (Oxford Univ. Press, New York 2005)

[44] S. Kobayashi, Y. Kawaguchi, M. Nitta and M. Ueda, Phys. Rev. **A86**, 023612 (2012)

[45] K. Fujimoto and M. Tsubota, Phys. Rev. **A85**, 053639 (2012); Phys. Rev. **A85**, 033642 (2012)

[46] M. Tsubota, Y. Aoki and K. Fujimoto, arXiv:1304.467v1 [2013]